International Journal of Nanomedicine

Dovepress
open access to scientific and medical research

Open Access Full Text Article

ORIGINAL RESEARCH

Porous Se@SiO_2 nanocomposite promotes migration and osteogenic differentiation of rat bone marrow mesenchymal stem cell to accelerate bone fracture healing in a rat model

This article was published in the following Dove Press journal:
International Journal of Nanomedicine

Chunlin Li[1,*]
Qi Wang[1,2,*]
Xiaohua Gu[3]
Yingjie Kang[4]
Yongxing Zhang[1]
Yangyang Hu[5]
Taixi Li[1]
Hansong Jin[1]
Guoying Deng[1]
Qiugen Wang[1]

[1]Trauma Center, Shanghai General Hospital, Shanghai Jiaotong University School of Medicine, Shanghai 201620, People's Republic of China; [2]Trauma Center, Shanghai General Hospital of Nanjing Medical University, Shanghai 200080, People's Republic of China; [3]Department of Orthopedics, Shanghai Seventh People's Hospital, Shanghai, 200137, People's Republic of China; [4]Department of Radiology, Shuguang Hospital, Shanghai University of Traditional Chinese Medicine, Shanghai 201203, People's Republic of China; [5]Department of Gastroenterology, Shanghai General Hospital, Shanghai Jiaotong University School of Medicine, Shanghai 201620, People's Republic of China

*These authors contributed equally to this work

Correspondence: Qiugen Wang; Guoying Deng
Trauma Center, Shanghai General Hospital, Shanghai Jiaotong University School of Medicine, 650 Xin Songjiang Road, Shanghai 201620, People's Republic of China
Tel +86 135 8556 1561
Fax +86 213 779 8527
Email wangqiugen@126.com; parisdeng2012@hotmail.com

Background: Delay or failure of bone union is a significant clinical challenge all over the world, and it has been reported that bone marrow mesenchymal stem cells (BMSCs) offer a promising approach to accelerate bone fracture healing. Se can modulate the proliferation and differentiation of BMSCs. Se-treatment enhances the osteoblastic differentiation of BMSCs and inhibiting the differentiation and formation of mature osteoclasts. The purpose of this study was to assess the effects of porous Se@SiO_2 nanocomposite on bone regeneration and the underlying biological mechanisms.

Methods: We oxidized Se^{2-} to develop Se quantum dots, then we used the Se quantum dots to form a solid Se@SiO_2 nanocomposite which was then coated with polyvinylpyrrolidone (PVP) and etched in hot water to synthesize porous Se@SiO_2 nanocomposite. We used XRD pattern to assess the phase structure of the solid Se@SiO_2 nanocomposite. The morphology of porous Se@SiO_2 nanocomposite were evaluated by scanning electron microscope (SEM) and the biocompatibility of porous Se@SiO_2 nanocomposite were investigated by cell counting kit-8 (CCK-8) assays. Then, a release assay was also performed. We used a Transwell assay to determine cell mobility in response to the porous Se@SiO_2 nanocomposite. For in vitro experiments, BMSCs were divided into four groups to detect reactive oxygen species (ROS) generation, cell apoptosis, alkaline phosphatase activity, calcium deposition, gene activation and protein expression. For in vivo experiments, femur fracture model of rats was constructed to assess the osteogenic effects of porous Se@SiO_2 nanocomposite.

Results: In vitro, intervention with porous Se@SiO_2 nanocomposite can promote migration and osteogenic differentiation of BMSCs, and protect BMSCs against H_2O_2-induced inhibition of osteogenic differentiation. In vivo, we demonstrated that the porous Se@SiO_2 nanocomposite accelerated bone fracture healing using a rat femur fracture model.

Conclusion: Porous Se@SiO_2 nanocomposite promotes migration and osteogenesis differentiation of rat BMSCs and accelerates bone fracture healing, and porous Se@SiO_2 nanocomposite may provide clinic benefit for bone tissue engineering.

Keywords: bone marrow mesenchymal stem cells, porous Se@SiO_2 nanocomposite, antioxidant, migration, osteogenic differentiation

Introduction

Delay or failure of bone union is a serious problem that troubles orthopedists, and it has been reported that more than 70% of all patients with major trauma require at

least one orthopedic surgery.[1] Approximately 5~10% of fractures result in delayed union or nonunion.[2] Bone marrow mesenchymal stem cells (BMSCs) offer a promising approach to accelerate bone fracture healing,[3] and recent studies have demonstrated encouraging results suggesting that BMSCs can promote bone fracture healing.[4] The capabilities of BMSCs to migrate to the fracture site, provide antioxidant protection and exhibit osteogenic differentiation play an important role in bone fracture healing.[5–7]

After bone fracture, the migration of endogenous BMSCs to the fracture sites is a crucial step in the maturation of osteoblasts and formation of mineralized tissue.[8,9] BMSCs migrate to the fracture site and then differentiate into osteoblasts and chondroblasts, which contribute to fracture healing through intramembranous ossification or endochondral ossification.[10,11] Hypoxia, which is caused by bone fracture and vascular injury, triggers BMSCs to express bone morphogenetic protein (BMP-2), allowing fracture healing to initiate.[12] However, the deficient scavenging of hypoxia-derived ROS impairs BMP-2 expression in BMSCs, and an abundance of ROS can also induce BMSCs apoptosis and restrain osteogenic differentiation,[13–15] which may result in the failed initiation of fracture healing and in fracture nonunion.

It has been reported that selenium (Se) can enhance immune surveillance, modulate the proliferation and differentiation of BMSCs and protect BMSCs against injury caused by oxidative stress,[16] and Se deficiency is detrimental to bone microarchitecture by increasing bone resorption.[17] In addition, at the cellular level, Se treatment enhances the osteoblastic differentiation of BMSCs by reducing basal oxidative stress[18] and inhibiting the differentiation and formation of mature osteoclasts.[19,20]

However, a high dose of Se is harmful to humans,[21] and Se has a narrow margin between safety and toxicity.[22] Therefore, using nanotechnology, we developed a porous Se@SiO_2 nanocomposite that can slowly release a beneficial amount of Se, and the controlled release and in vivo stability of the porous Se@SiO_2 nanocomposite provide the characteristics of biosafety and low toxicity.[23]

We used hydrogen peroxide (H_2O_2) to induce oxidative stress, and using an Annexin V- fluorescein isothiocyanate (FITC) / propidium iodide (PI) assay and a TUNEL assay, we found that the porous Se@SiO_2 nanocomposite can reduce oxidative stress induced by H_2O_2 and protect BMSCs against H_2O_2-induced apoptosis. We detected that the porous Se@SiO_2 nanocomposite can protect BMSCs against H_2O_2-induced inhibition of osteogenic differentiation by measuring alkaline phosphatase (ALP) activity and staining with Alizarin Red S, which suggested that the porous Se@SiO_2 nanocomposite can protect BMSCs from osteogenic inhibition induced by H_2O_2 in the early and late stages of differentiation. Osteogenic differentiation of BMSCs into mature osteoblast is a complex process, and there are a number of transcriptional factors that participate in this process, including runt-related transcription factor 2 (Runx2) and BMPs. Runx2 is a transcription factor that plays an important role in osteogenic differentiation, and mice lacking Runx2 showed a complete lack of ossification.[24] BMPs can phosphorylate Smad1, Smad5 and Smad9 and then phosphorylated Smad1, phosphorylated Smad5 and phosphorylated Smad9 form a complex with Smad4. The complex translocated into the nucleus and interacts with Runx2 to initiate osteogenic differentiation. We found that the porous Se@SiO_2 nanocomposite promotes osteogenic differentiation of BMSCs through the BMP/Smad signaling pathway and that Runx2 participates in this process. It has been reported that the stromal cell-derived factor-1 (SDF-1)/CXC chemokine receptor-4 (CXCR4) signaling pathway controls BMSCs migration and that enhanced CXCR4 expression can improve the migration capacity of BMSCs.[25,26] We were pleasantly surprised to find that the porous Se@SiO_2 nanocomposite promotes migration of BMSCs using a Transwell assay. We detected enhanced gene expression of SDF-1 and CXCR4, indicating that the effects of the porous Se@SiO_2 nanocomposite on BMSC migration may be mediated by the SDF-1/CXCR4 signaling pathway. Finally, using a rat femur fracture models, we demonstrated that the porous Se@SiO_2 nanocomposite accelerated bone fracture healing in vivo.

In this study, we demonstrated that the application of a porous Se@SiO_2 nanocomposite protected BMSCs against H_2O_2-induced apoptosis. In addition, the porous Se@SiO_2 nanocomposite also promoted osteogenic differentiation of BMSCs and protected BMSCs against H_2O_2-induced inhibition of osteogenic differentiation through the BMP/Smad signaling pathway. We found that the porous Se@SiO_2 nanocomposite promoted BMSC migration using a transwell assay, and the SDF-1/CXCR4 signaling pathway might play an important role in this process. Using a rat femur fracture models, we demonstrated that the porous Se@SiO_2 nanocomposite can accelerate bone fracture healing in vivo.

Materials and methods

Synthesis and characterization of porous Se@SiO_2 nanocomposites

We synthesize a porous Se@SiO_2 nanocomposites according to our previous study.[23] First, we oxidized Se^{2-} to develop Se quantum dots. Next, the Se quantum dots were used to form a solid Se@SiO_2 nanocomposites in an alkaline environment. Then, the solid Se@SiO_2 nanocomposites were coated with polyvinylpyrrolidone (PVP) and etched in hot water to synthesize porous structures. We also characterized Se@SiO_2 nanocomposites by means of a D/max-2550 PC X-ray diffractometer (XRD, Cu–Kα radiation; Rigaku; Tokyo, Japan) and transmission electronic microscopy (TEM; JEM-2100F; JEOL, Tokyo, Japan). Finally, we detected the cumulative release kinetics of Se from the porous Se@SiO_2 nanocomposites in PBS at pH 7.4 and 37°C. Five milligrams of the porous Se@SiO_2 nanocomposites was dispersed with ultrasonication in 2.5 mL of PBS of pH 7.4. Subsequently, the mixture was shaken at 37°C. At various time intervals, the mixtures were centrifuged to obtain supernatant, which was replaced with fresh PBS. The supernatant was filtered at various times, and the contents of released Se were determined by a Leeman ICP-AES Prodigy instrument.

Cell culture and animals

All experiments were approved by the Experimental Animal Center of Shanghai Jiao Tong University. The rats were bred and maintained under a 12/12 hr light/dark cycle with free access to food and water. The temperature was maintained at 18–25°C, and the relative humidity was set to 40–60%. Rats were housed for 1 week before the experiments began. BMSCs were derived from Sprague Dawley (SD) rats, which were approximately 100 g. Briefly, BMSCs were isolated from an aspirate of bone marrow that was harvested from the tibia and femur marrow compartment. Then, the complex was cultured in DMEM/F12 essential medium (HyClone, Logan City, Utah, USA) with 10% FBS (Gibco, Grand Island, New York, USA) and 1% antibiotic–antimycotic (Gibco, Grand Island, New York, USA) for 48 hrs at 37°C with 5% CO_2. The detailed procedures for isolating BMSCs have been previously published.[27] Nonadherent cells were removed after 48 hrs, and fresh medium was added. When the cultures were almost 80% confluent, the cells were treated with 2 mL of 0.25% trypsin containing 0.02% EDTA (Gibco) for 2 mins at 37°C. Then, we cultured all lifted cells in a 10-cm cell culture dish, discarded the nonlifted cells and changed the culture medium every 3 days (using 9 mL of fresh medium each time). BMSCs from passages 3–4 were used in the following experiments.

In vitro safety of Se@SiO_2 nanocomposites

We evaluated the in vitro safety of the porous Se@SiO_2 nanocomposite by determining its inhibitory effect on BMSCs proliferation. BMSCs were seeded at a density of 1×10^4 cells per well in a flat-bottomed 96-well plate for 24 hrs at 37°C with 5% CO_2. After 24 hrs, the cells were incubated with an increasing concentration of the porous Se@SiO_2 nanocomposite (ranging from 0 to 180 μg/mL). The next day, the proliferation of cells was determined by a CCK-8 (Yeasen Biological Technology, Shanghai, China) according to the manufacturer's instructions, and the results were read using a microplate reader (Thermo Fisher Scientific, Multiskan GO, Waltham, MA, USA).

In vitro migration assays

We used a transwell assay (Costar, Transwell, Corning, New York, NY, USA), which was performed in 24-well transwell chambers with 8 μm nitrocellulose pore filters, to evaluate the effect of the porous Se@SiO_2 nanocomposite on BMSCs migration. BMSCs were divided into two groups: the blank group and the Se@SiO_2 group. The blank group was resuspended in serum-free DMEM/F12 medium, and the Se@SiO_2 group was resuspended in serum-free DMEM/F12 medium containing the porous Se@SiO_2 nanocomposite at a concentration of 80 μg/mL. Then, the BMSCs were loaded into the upper chamber, and DMEM/F12 medium containing 10% FBS was placed in the lower chamber. After 16 hrs, the BMSCs that passed through the membranes of the upper chambers were fixed with 4% paraformaldehyde (Servicebio, Wuhan, Hubei, China) and stained with 1% crystal violet dye solution (Beyotime Biotechnology, Shanghai, China) before images of each group were captured using a microscope (Leica, Leica DMi8, Heidelberg, Germany).

Detection of ROS and analysis of cell apoptosis

The BMSCs were seeded in 6-well plates and divided into four groups: the blank group, the H_2O_2 group (H_2O_2 at a concentration of 100 μM), the H_2O_2+ Se@SiO_2 group (H_2O_2 at a concentration of 100 μM and the porous Se@SiO_2 nanocomposite at a concentration of 80 μg/mL) and the H_2O_2+ Se@SiO_2 group (H_2O_2 at a concentration of 100 μM and the

porous Se@SiO_2 nanocomposite at a concentration of 160 μg/mL). After 24 hrs of treatment, we used 2, 7-Dichlorodihydrofluorescein diacetate (DCFH-DA) (Yeasen Biotech) to measure intracellular ROS. After DCFH-DA treatment according to the manufacturer's instructions, the BMSCs were washed three times with PBS. Then, we acquired images using a fluorescence microscope (Leica, Leica DMi8). BMSCs apoptosis was detected using an Annexin V-FITC/PI Kit (Invitrogen, Waltham, MA, USA) and TUNEL Kit (Yeasen Biotech). For the Annexin V-FITC/PI assay, briefly, BMSCs were washed with PBS and binding buffer and then resuspended in 200 μL of binding buffer containing 10 μL of Annexin V for 15 mins on ice in the dark. Then, PI was added to the binding buffer and the cells were stained for 5 mins. BMSCs apoptosis was immediately analyzed by flow cytometry (BD, AccuriTM C6, Franklin Lakes, NJ, USA). Approximately 10,000 cells were analyzed in each sample. For the TUNEL assay, briefly, the fixed BMSCs on the slides were washed with PBS and permeabilized with Triton X-100 (Beyotime Biotechnology) for 2 mins, followed by incubation with 50 μL of TUNEL reaction mixture according to the manufacturer's instructions. Finally, the nuclei were stained with DAPI (Beyotime Biotechnology) and observed under a fluorescence microscope (Leica, Leica DMi8).

Osteogenic differentiation

The BMSCs were plated in a 24-well plate at a concentration of 2×10^4 cells/cm^2 and divided into four groups: the blank group, the Se@SiO_2 group, the H_2O_2 group and the H_2O_2+ Se@SiO_2 group. When the cultures were almost 60–70% confluent, the medium of the blank group was replaced with osteogenic induction medium (OIM) (Cyagen Biosciences Inc, Santa Clara, CA, USA), and the medium of the Se@SiO_2 group was replaced with OIM containing Se@SiO_2 at a concentration of 80 μg/mL. The medium of the H_2O_2 group was replaced by OIM with H_2O_2 at a concentration of 100 μM, and the medium of the H_2O_2+ Se@SiO_2 group was replaced by OIM with 100 μM H_2O_2 and 80 μg/mL porous Se@SiO_2 nanocomposite. After 7 days of osteogenic induction, ALP activity of the four different groups was measured. The BMSCs were washed three times with PBS, fixed with 4% paraformaldehyde (Servicebio, Wuhan, Hubei, China) and stained with a BCIP/NBT Alkaline Phosphatase Color Development Kit (Beyotime Biotechnology) according to the manufacturer's instructions. Alizarin Red S (Cyagen Biosciences Inc) staining was used to assess the mineralization of the different groups. After 21 days of osteogenic induction, the BMSCs were washed three times with PBS, fixed with 4% paraformaldehyde (Servicebio, Wuhan, Hubei, China) and incubated in 1% Alizarin Red S (Cyagen Biosciences Inc) for 30 mins. Images of calcium deposition were captured using a microscope (Leica, Leica DMi8) after washing three times with PBS.

Western blot

The BMSCs were plated in a 6-well plate at a concentration of 2×10^4 cells/cm^2 and divided into four groups: the blank group, the Se@SiO_2 group, the H_2O_2 group and the H_2O_2+ Se@SiO_2 group. After 7 days of osteogenic induction, the BMSCs were washed three times with PBS and lysed in lysis buffer (Biotech Well, Shanghai, China) containing protease inhibitors (Biotech Well), phosphatase inhibitors (Biotech Well) and phenylmethanesulfonyl fluoride (PMSF) (Biotech Well). Protein concentration was determined using a bicinchoninic acid (BCA) protein assay kit (Biotech Well). Equal amounts of protein from each group were denatured and electrophoresed and then transferred to a cellulose acetate membrane. After blocking in 5% nonfat milk for 2 hrs with rocking, the membrane was incubated in primary antibodies including anti-pSmad1/pSmad5/pSmad9 (Cell Signaling Technology, phospho-Smad1/Smad5/Smad9 Rabbit mAb, 1:1,000 dilution, Danvers, MA, USA), anti-Smad1/Smad5/Smad9 (Abcam, Smad1/Smad5/Smad9, 1:1,000 dilution, Cambridge, UK) and anti-β-actin (Proteintech, anti-β-actin, 1:5,000 dilution, Wuhan, Hubei, China) at 4°C overnight and then incubated in the corresponding secondary antibody (LI-COR, goat anti-mouse IgG (H + L)/goat anti-rabbit IgG (H + L), Lincoln, NE, USA) at room temperature for 2 hrs. After being washed three times with Tris-buffered saline (TBS) (Sangon Biotech, Shanghai, China), the cellulose acetate membrane was detected with fluorography (LI-COR, Odyssey CLX, Lincoln, NE, USA).

Immunofluorescence staining

BMSCs of the blank group, the Se@SiO_2 group, the H_2O_2 group and the H_2O_2+ Se@SiO_2 group were fixed in 4% paraformaldehyde (Servicebio, Wuhan, Hubei, China), washed with PBS, permeabilized with 1% Triton X-100 (Beyotime Biotechnology) for 30 mins and then blocked in 1% BSA (Kingmorn, Shanghai, China). Next, the cells were immunostained with primary antibodies (anti-pSmad1/pSmad5/pSmad9) (Cell Signaling Technology, phospho-Smad1/Smad5/Smad9 Rabbit mAb, 1:800 dilution), followed by Cy3-labeled goat anti-rabbit IgG (H + L)

(Biotech Well). Finally, the cells were covered with an antifade reagent (Biotech Well) and observed under a confocal microscope (Leica, Leica TCS SP8).

Total RNA extraction and real-time reverse transcription polymerase chain reaction (RT-PCR)

The BMSCs were plated in a 6-well plate at a concentration of 2×10^4 cells/cm^2 and divided into four groups: the blank group, the Se@SiO_2 group, the H_2O_2 group and the H_2O_2+ Se@SiO_2 group. After 7 days of osteogenic induction, the transcript levels of genes associated with osteogenic differentiation, including *Runx2*, *osteocalcin* (*OCN*), *BMP*-2 and *Smad-1*, were evaluated. After 16 hrs of treatment with Se@SiO_2, we evaluated the transcript levels of *SDF-1* and *CXCR4* in the blank and Se@SiO_2 groups. We used Primer Premier 5 (PREMIER Biosoft International, Palo Alto, CA, USA) to design the primers. Total cellular RNA was extracted with RNeasy (Biotech Well) according to the manufacturer's instructions. PCR amplification was performed using the ABI StepOne Plus System (Applied Biosystems, Waltham, MA, USA), and the primer sequences that were determined from established GenBank sequences are listed in Table 1. *β-Actin* was used as an internal control to evaluate the relative expression. The relative transcript levels were calculated as ΔC = Ctct1 − CtGAPDH.

Rat femur fracture model and analysis

Male SD rats with a weight range of 250–300 g were used in the study. We made an incision at the level of the lateral condyle, distally over the lateral right femur and separated the gluteus superficialis and biceps femoris muscles to expose the femur. We used a sagittal saw to make a transverse osteotomy at the middle part of the femur. An intramedullary 1.1 mm, Kirschner wire was inserted at the osteotomy and passed through the knee. Then, the Kirschner wire was cut at the level of the articular surface of the knee. Finally, the incision was closed with an absorbable suture. Next, the SD rats were randomly divided into the blank group (n=10) and the Se@SiO_2 group (n=10). The rats in the Se@SiO_2 group were injected intraperitoneally with the porous Se@SiO_2 nanocomposite (1 mg/kg) per day, and the rats in the blank group were injected with saline. In addition, each rat was administered penicillin intramuscularly for 7 days after the operation to prevent infection, and the rats were housed under identical conditions. Callus formation and bridging bone formation at the fracture site were monitored using a digital X-ray machine (Siemens, Munich, Germany) at 2–6 wk postoperatively. Radiographs of each animal were assessed by two independent observers. Rats were sacrificed, and the femurs were harvested for micro-CT (SCANCO Medical AG, Zurich, Switzerland) analysis at 6 weeks after operation. The scan ranges from 3 mm proximal to the fracture line to 3 mm distal to the fracture line. The animal experimental protocol was in accordance with the guidelines of the National Institutes of Health Guide for the Care and Use of Laboratory Animals, and the animal experiment was approved by the Ethics Committee of Shanghai General Hospital.

Statistical analysis

All experiments were performed at least three times. Qualitative data were representative of at least three independent experiments. Quantitative or semiquantitative data were expressed as means ± SD. The data were analyzed using GraphPad Prism 6 (Graphpad Software Inc, La Jolla, CA, USA). The differences of data between two groups were determined by two-tailed unpaired or paired *t*-tests and $P<0.05$ was considered to be significantly different.

Table 1 Primers used in RT-PCR

Gene	Forward primer sequence (5′–3′)	Reverse primer sequence (5′–3′)
Runx2	CCTGAACTCAGCACCAAGTCCT	TCAGAGGTGGCAGTGTCATCA
OCN	AATAGACTCCGCGCTACCTC	GCTAGCTCGTCACAATTGGG
SDF-1	CTCTGCATCAGTGACGGTAAGC	GGATTTTCAGATGTTTGACGTTGG
CXCR4	CATCTGTGACCGCCTTTACCC	GACGCTCTCGAACTCACATCC
BMP-2	CCTATATGCTCGACCTGTACCG	CTGGCTGTGGCAGGCTTTAT
Smad-1	AAGCCTCTGGAATGCTGCGA	GCTCATTTTGTCCCAGGTTTCG
GADPH	CAAGTTCAACGGCACAGTCA	CCCCATTTATGTTAGCGGG

Abbreviation: RT-PCR, real-time reverse transcription polymerase chain reaction.

Results

Characterization of the porous Se@SiO_2 nanocomposites

The phase structure of the solid Se@SiO_2 nanocomposites was assessed using an XRD pattern, which showed an increase in the low-angle region. The characteristic peaks of the solid Se@SiO_2 nanocomposites exhibited a hexagonal phase, as referenced by the standard Se phase (Figure 1A).

We used TEM to detect the morphological characteristics and sizes of the Se@SiO_2 nanocomposites. The solid Se@SiO_2 nanocomposites are shown in Figure 1B and Figure 1C, and the porous Se@SiO_2 nanocomposites are shown in Figure 1D. As we can see, irregular quantum dots were interspersed from the center to the surface, the size of which was <5 nm (Figure 1B, C).

We also used a CCK-8 assay to evaluate the cytotoxicity of the Se@SiO_2 nanocomposites on BMSCs according to the manufacturer's instructions. BMSCs were incubated with the porous Se@SiO_2 nanocomposite at a concentration of 0–180 μg/mL, and the results showed that the cell viability did not decrease significantly compared to the cell viability of the blank group until the concentration reached 160 μg/mL (Figure 1E).

Se release was measured at pH 7.4 and 37°C, which is close to semiphysiological conditions. As shown in Figure 1F, the release rate of Se was rapid on the first day and gradually slowed over the next 9 days (Figure 1F), and the results were consistent with those in our previous study.[28,29]

The porous Se@SiO_2 nanocomposite promotes BMSCs migration

The migration of BMSCs was assessed in vitro. We used a transwell assay to determine cell mobility in response to the porous Se@SiO_2 nanocomposite. Our results

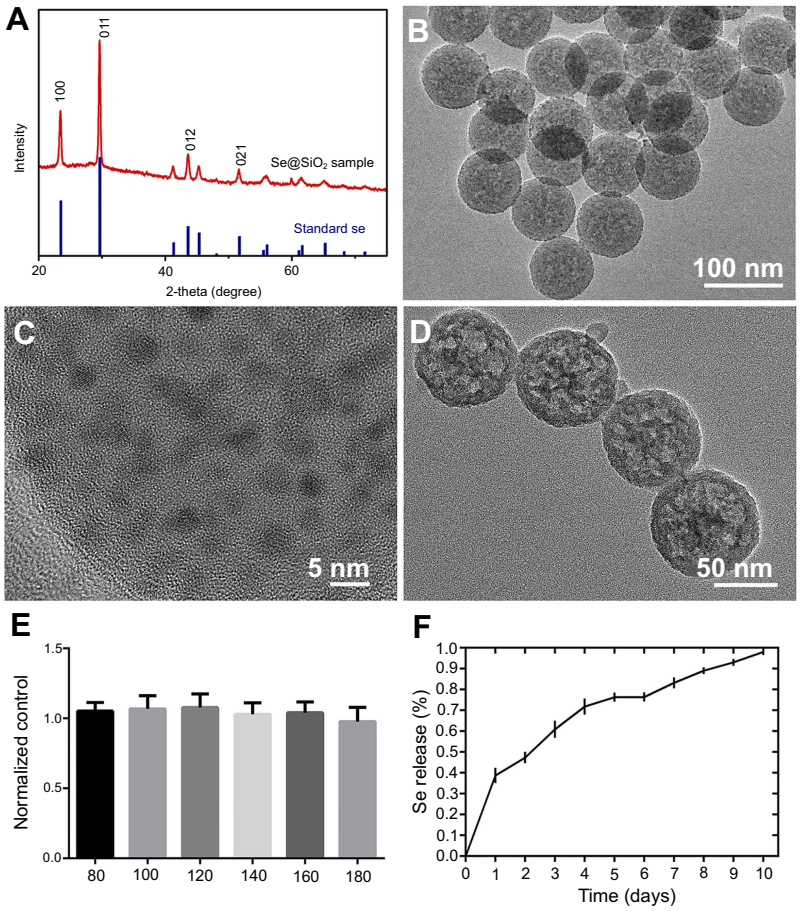

Figure 1 The characterization and cytotoxicity of the Se@SiO_2 nanocomposites. (**A**) XRD pattern of the solid Se@SiO_2 nanocomposites and the standard hexagonal phase of Se (JCPDS card no: 65-1876). (**B**) Low- and (**C**) high-magnification TEM image of the solid Se@SiO_2 nanocomposites. (**D**) Medium-magnification images of the porous Se@SiO_2 nanocomposites. (**E**) The cell viability of BMSCs treated with different concentrations of the porous Se@SiO_2 nanocomposites for 24 hrs. Data are expressed as means ± SDs (n=3). (**F**) The cumulative release kinetics of Se from the porous Se@SiO_2 nanocomposites in PBS at 37°C and pH 7.4.
Abbreviations: TEM, transmission electron microscopy; XRD, X-ray diffractometer.

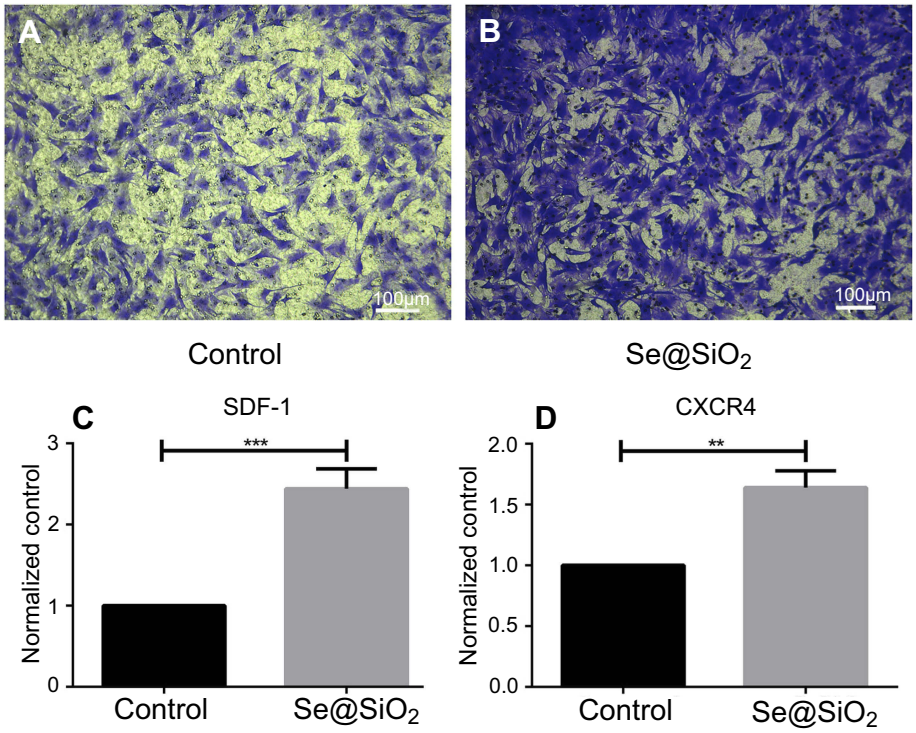

Figure 2 Porous Se@SiO_2 nanocomposite has a powerful capacity to promote BMSCs migration. (**A** and **B**) The porous Se@SiO_2 nanocomposite can promote migration of BMSCs, which was demonstrated by transwell assays. BMSCs that passed through the membrane were detected with crystal violet staining. (**C**) The gene expression of SDF-1 in the blank group and Se@SiO_2 group was compared using RT-PCR. ***p<0.05, blank group vs Se@SiO_2 group. Data are expressed as means ± SDs (n=3). (**D**) The gene expression of CXCR4 in the blank group and Se@SiO_2 group. **p<0.05, blank group vs Se@SiO_2 group. All data were expressed as mean ± SDs (n=3).
Abbreviation: BMSCs, bone marrow mesenchymal stem cells.

demonstrated that the porous Se@SiO_2 nanocomposite promoted BMSCs migration compared to that in the blank group (Figure 2A, B). Then, we compared the mRNA expression levels of the blank group and the Se@SiO_2 group. We found that the gene expression of SDF-1 and CXCR4 in the Se@SiO_2 group was increased compared to that in the blank group, suggesting that the porous Se@SiO_2 nanocomposite may promote BMSCs migration through the SDF-1/CXCR4 signaling pathway (Figure 2C, D).

The porous Se@SiO_2 nanocomposite reduces intracellular ROS formation and protects BMSCs against H_2O_2-induced apoptosis

To explore the effects of the porous Se@SiO_2 nanocomposite on ROS generation, we detected ROS using fluorescent dichlorofluorescein (DCF) after H_2O_2 treatment. Compared with the blank group, H_2O_2 led to a significant increase in DCF fluorescence. Treatment with the porous Se@SiO_2 nanocomposite significantly decreased the level of intracellular ROS, and porous Se@SiO_2 nanocomposite decreased the level of intracellular ROS more evidently at 160 μg/mL than at 80 μg/mL (Figure 3A–D, and U). We assessed BMSCs apoptosis by an Annexin V and PI double-staining. BMSCs labeled with Annexin V (Annexin V^+) indicate apoptotic cells, including early apoptotic cells (Annexin V^+/PI^-) and late apoptotic cells (Annexin V^+/PI^+). The percentage of apoptotic cells was 0.1% in the control group. After H_2O_2 treatment, the percentage of apoptotic cells increased to 88.8%. After treatment with 80 μg/mL and 160 μg/mL porous Se@SiO_2 nanocomposite, the percentage of apoptotic cells decreased to 34.1%, and 14.1%, respectively (Figure 3E–H, V, and W). We also used a TUNEL assay to detect the apoptosis rate of BMSCs. The results showed that the increased apoptosis rate in the H_2O_2 group was comparable to that in the blank group, and the apoptosis rate in the H_2O_2+ Se@SiO_2 group (the concentration of porous Se@SiO_2 nanocomposite was 80 μg/mL and 160 μg/mL, respectively) was significantly lower than that in with the H_2O_2 group. The porous Se@SiO_2 nanocomposite at a concentration of 160 μg/mL decreased the apoptosis rate more evidently than did the porous Se@SiO_2 nanocomposite at a concentration of 80 μg/mL, which further demonstrates that the porous

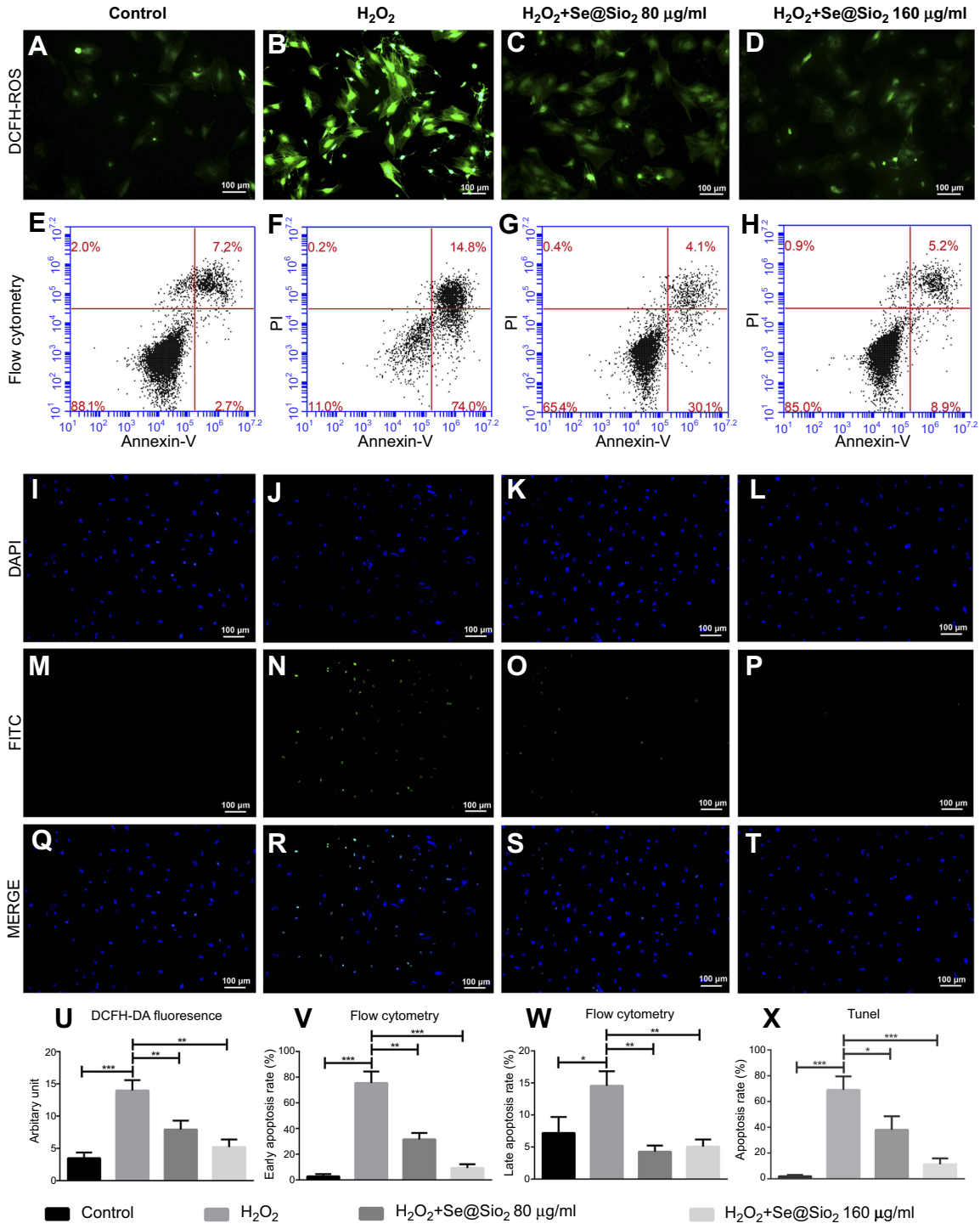

Figure 3 Porous Se@SiO_2 nanocomposite can reduce intracellular ROS formation and protect BMSCs against hydrogen peroxide-induced apoptosis. (**A**–**D**) The production of ROS induced by H_2O_2 in the H_2O_2 group was higher than that in the H_2O_2+ Se@SiO_2 group, and the porous Se@SiO_2 nanocomposite at a concentration of 160 μg/mL could decrease the level of intracellular ROS more than porous Se@SiO_2 nanocomposite at a concentration of 80 μg/mL. (**E**–**H**) Cell apoptosis was detected by flow cytometry analysis after staining with Annexin V and PI. (**I**–**T**) Staining BMSCs with DAPI and TUNEL. (**U**) Staining of BMSCs with ROS and DAPI, ***p<0.05, blank group vs H_2O_2 group, **p<0.05, H_2O_2 group vs H_2O_2+ Se@SiO_2 group (80 μg/mL), **p<0.05, H_2O_2 group vs H_2O_2+ Se@SiO_2 group (160 μg/mL). Data are expressed as means ± SDs (n=3). (**V**) The bar graph of early apoptosis rate (%), ***p<0.05, blank group vs H_2O_2 group, **p<0.05, H_2O_2 group vs H_2O_2+ Se@SiO_2 group (80 μg/mL), ***p<0.05, H_2O_2 group vs H_2O_2+ Se@SiO_2 group (160 μg/mL). Data are expressed as means ± SDs (n=3). (**W**) The bar graph of late apoptosis rate (%), *p<0.05, blank group vs H_2O_2 group, **p<0.05, H_2O_2 group vs H_2O_2+ Se@SiO_2 group (80 μg/mL), **p<0.05, H_2O_2 group vs H_2O_2+ Se@SiO_2 group (160 μg/mL). Data are expressed as means ± SDs (n=3). (**X**) Statistical analysis of TUNEL staining. The numbers of TUNEL-positive cells of all cells was calculated under a fluorescent microscope. ***p<0.05, blank group vs H_2O_2 group, *p<0.05, H_2O_2 group vs H_2O_2+ Se@SiO_2 group (80 μg/mL), ***p<0.05, H_2O_2 group vs H_2O_2+ Se@SiO_2 group (160 μg/mL). All data are expressed as means ± SDs (n=3).

Abbreviations: ROS, reactive oxygen species; DCF, dichlorofluorescein; DAPI, 4',6-diamidino-2-phenylindole; FITC, fluorescein isothiocyanate; PI, propidium iodide.

$Se@SiO_2$ nanocomposite can protect BMSCs against H_2O_2-induced apoptosis (Figure 3I–T and X).

The porous $Se@SiO_2$ nanocomposite promotes osteogenic differentiation of BMSCs and protects BMSCs against H_2O_2-induced inhibition of osteogenic differentiation through the BMP/Smad signaling pathway

After 7 days of osteogenic induction, we measured the ALP activity of four different groups and found that the porous $Se@SiO_2$ nanocomposite increased ALP activity in the $Se@SiO_2$ group and the H_2O_2+$Se@SiO_2$ group compared with that in the blank group and the H_2O_2 group, respectively (Figure 4A–H). After 21 days of osteogenic induction, BMSCs were incubated in 1% Alizarin Red S for 30 mins, and we found that more calcium deposits appeared in the $Se@SiO_2$ group and H_2O_2+$Se@SiO_2$ group than in the blank group and H_2O_2 group (Figure 4I–P). Because of its important role in osteogenic differentiation, we hypothesized that the BMP/Smad signaling pathway might be involved in osteogenic differentiation induced by the porous $Se@SiO_2$ nanocomposite. After 7 days of osteogenic induction, the mRNA levels of Runx2, OCN, BMP-2 and Smad-1 were analyzed using RT-PCR analysis (Figure 4Q–T). We found that the porous $Se@SiO_2$ nanocomposite promoted the expression of *Runx2, OCN, BMP-2* and *Smad-1* using RT-PCR and protected the expression of *Runx2, OCN, BMP-2* and *Smad-1* against H_2O_2-induced inhibition, suggesting that the porous $Se@SiO_2$ nanocomposite promotes osteogenic differentiation of BMSCs and that the BMP/Smad signaling pathway may be involved in this process. Then, we used Western blot to detect the effects of porous $Se@SiO_2$ nanocomposite on pSmad1/5/9 and Smad1/5/9 protein levels. Western blot analysis showed that the porous $Se@SiO_2$ nanocomposite increased the levels of pSmad1/5/9 but had no obvious effects on the total protein levels of Smad1/5/9, suggesting that the BMP/Smad signaling pathway may participate in osteogenic differentiation induced by the porous $Se@SiO_2$ nanocomposite (Figure 4U–X). To further study the influence of the porous $Se@SiO_2$ nanocomposite on the BMP/Smad signaling pathway, we detected the nuclear translocation of pSmad1/5/9, which acts as an activator of the BMP/Smad signaling pathway. The results of our study showed that the porous $Se@SiO_2$ nanocomposite promoted pSmad1/5/9 translocation from the cytoplasm to the nucleus (Figure 5A–X). In summary, we suggest that the porous $Se@SiO_2$ nanocomposite can promote osteogenic differentiation and protect BMSCs against H_2O_2-induced inhibition of osteogenic differentiation through the BMP/Smad signaling pathway, and Runx2, which is an important transcription factor responsible for the osteogenic differentiation of BMSCs, is involved in this process.

The porous $Se@SiO_2$ nanocomposite promotes fracture healing in a rat femur fracture model

We created an open femur fracture model using 8-week-old male SD rats to explore whether the porous $Se@SiO_2$ nanocomposite could accelerate bone fracture healing. The radiographs of the $Se@SiO_2$ group showed that bridging callus formation was observed at 2 weeks after porous $Se@SiO_2$ nanocomposite injection. In addition, the cortical gap of the $Se@SiO_2$ group disappeared at 4 weeks, which indicated bone union. In contrast, the bridging callus formation of the blank group was observed at 4 weeks, and the cortical gap of the blank group disappeared at 6 weeks (Figure 6A–F). Six weeks after injection, we collected the femurs for micro-CT (Figure 7A–F). According to the micro-CT results, there was more bone formation in the $Se@SiO_2$ group than in the blank group, and the bone mineral density (BMD) (Figure 7G) and total bone volume (BV)/total tissue volume (TV) (Figure 7H) were higher than those of the blank group.

Our results suggest a working model of the porous $Se@SiO_2$ nanocomposite for the promotion of osteogenic differentiation and protection of BMSCs against H_2O_2-induced inhibition of osteogenic differentiation, as shown in Figure 8. In this model, the porous $Se@SiO_2$ nanocomposite can activate the BMP/Smad signaling pathway by increasing the levels of phosphorylated Smad1/5/9. Then, phosphorylated Smad1, phosphorylated Smad5 and phosphorylated Smad9 can form a complex with Smad4, and this complex translocates into the nucleus. In the nucleus, phosphorylated Smads proteins (pSmad) can increase the expression of osteogenic differentiation genes, such as *Runx-2*, to promote the osteogenic differentiation of BMSCs.

Discussion

In this study, we found that the porous $Se@SiO_2$ nanocomposite promotes BMSCs migration and protects BMSCs against H_2O_2-induced apoptosis. In addition, the porous $Se@SiO_2$ nanocomposite also protects BMSCs

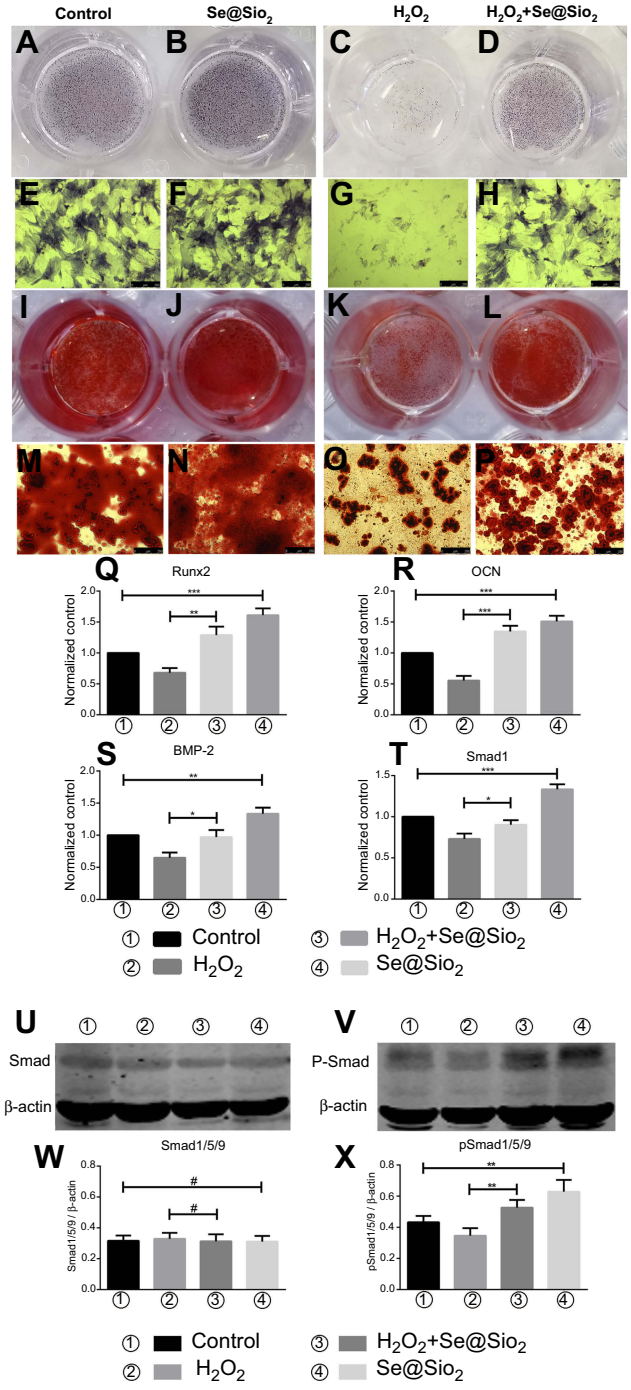

Figure 4 Porous Se@SiO_2 nanocomposite can promote osteogenic differentiation of BMSCs and protect BMSCs against H_2O_2-induced inhibition of osteogenic differentiation through the BMP/Smad signaling pathway. (**A**–**H**) The ALP activity of each group was measured after 7 days. (I–**P**) Calcium deposits of each group were measured by Alizarin Red staining after 21 days. (**Q**–**T**) After 7 days of osteogenic induction, the genes of each group related to osteogenic differentiation of BMSCs were analyzed by RT-PCR. (**Q**) Porous Se@SiO_2 nanocomposite increased the expression of *Runx2*. ***p<0.05, blank group vs Se@SiO_2 group, **p<0.05, H_2O_2 group vs H_2O_2+ Se@SiO_2 group. (**R**) Porous Se@SiO_2 nanocomposite increased the expression of *OCN*. ***p<0.05, blank group vs Se@SiO_2 group, ***p<0.05, H_2O_2 group vs H_2O_2+ Se@SiO_2 group. (**S**) Porous Se@SiO_2 nanocomposite increased the expression of *BMP-2*. **p<0.05, blank group vs Se@SiO_2 group, *p<0.05, H_2O_2 group vs H_2O_2+ Se@SiO_2 group. (**T**) Porous Se@SiO_2 nanocomposite increased the expression of *Smad1*. ***p<0.05, blank group vs Se@SiO_2 group, *p<0.05, H_2O_2 group vs H_2O_2+ Se@SiO_2 group. (**U** and **V**) Total proteins from four groups were extracted, and we analyzed the levels of Smad1/5/9 and pSmad1/5/9 by Western blot. **β**-Actin was used as a loading control. (**W**) Expression of Smad1/5/9 was determined by Western blotting. There was no significant difference of blank group vs Se@SiO_2 group and H_2O_2 group vs H_2O_2+ Se@SiO_2 group, $^{\#}p$>0.05. (**X**) Expression of pSmad1/5/9 was determined by Western blotting. **p<0.05, blank group vs Se@SiO_2 group, **p<0.05, H_2O_2 group vs H_2O_2+ Se@SiO_2 group. All data are expressed as means ± SDs (n=3).

Abbreviations: ALP, alkaline phosphatase; ARS, Alizarin Red s.

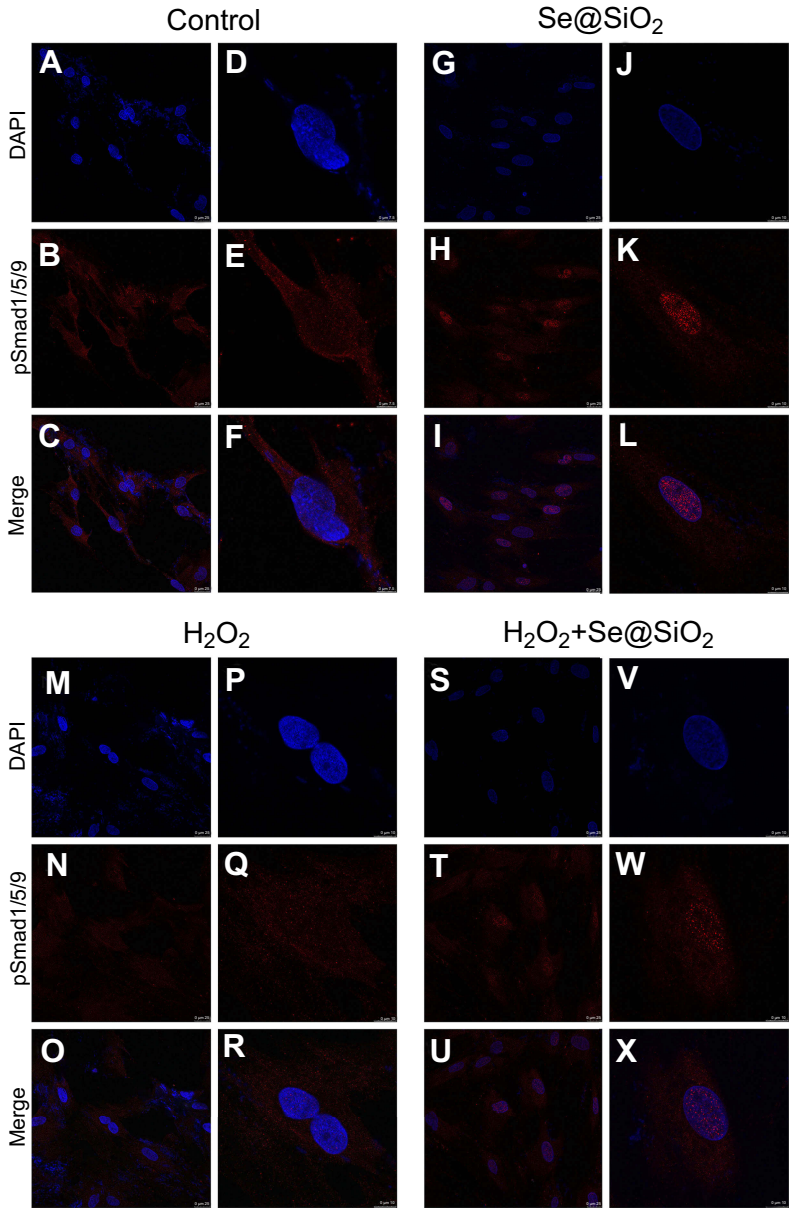

Figure 5 Porous $Se@SiO_2$ nanocomposite promoted the translocation of pSmad1/5/9 from the cytoplasm to the nucleus. (**A**–**X**) Immunofluorescence analysis of pSmad1/5/9 in four different groups.
Abbreviation: DAPI, 4',6-diamidino-2-phenylindole.

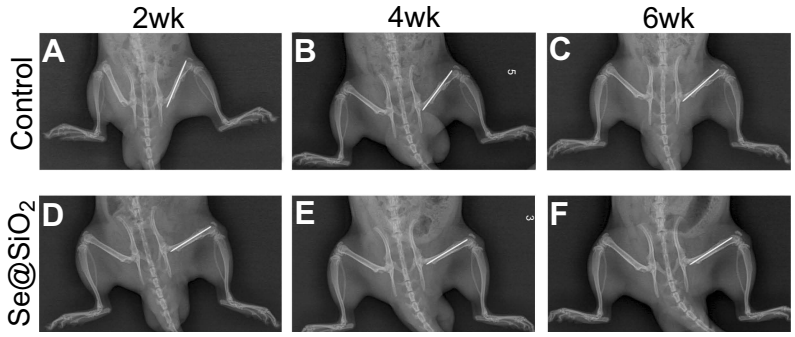

Figure 6 Radiographs at 2, 4 and 6 weeks were taken after the operation. (**A**–**F**) The bridging callus formation was observed at 2 weeks after operation in the $Se@SiO_2$ group. The cortical gap of the $Se@SiO_2$ group disappeared at 4 weeks postoperatively. On the other hand, bridging callus formation in the blank group was observed at 4 weeks, and there was no bone union at 4 weeks. All data are expressed as means ± SDs (n=3).

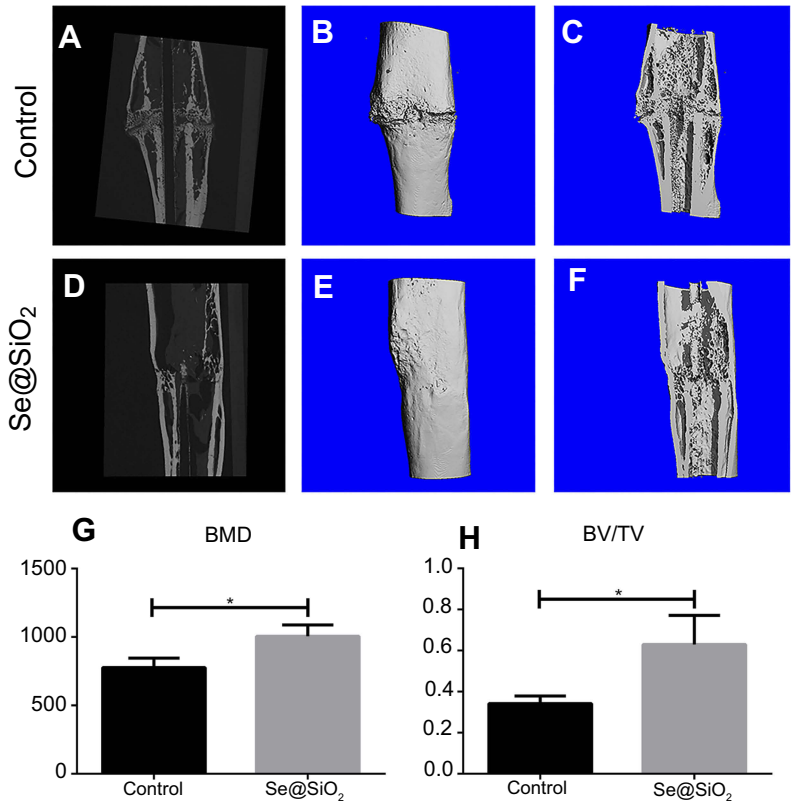

Figure 7 The results of micro-CT of fracture callus at 6 weeks after operation. (**A**–**F**) Representative images of micro-CT of the Se@SiO_2 group and blank group. (**G**) The BMD was analyzed by micro-CT. *p<0.05, blank group vs Se@SiO_2 group. (**H**) The BV/TV was analyzed by micro-CT. *p<0.05, blank group vs Se@SiO_2 group.
Abbreviations: CT, computed tomography; BMD, bone mineral density; BV, bone volume; TV, tissue volume.

against H_2O_2-induced inhibition of osteogenic differentiation and promotes bone fracture healing in SD rats.

The migration of endogenous BMSCs to the fracture site is critical for bone fracture healing, which contributes to osteoblast maturation and the formation of mineralized tissue through intramembranous ossification or endochondral ossification.[30] Apart from direct cell differentiation, BMSCs can also promote bone fracture healing by secreting different kinds of growth factors and inflammatory cytokines.[31–33] We indicated that the porous Se@SiO_2 nanocomposite can promote BMSCs migration in vitro using a transwell assay. We detected that the gene expression of *SDF-1* and *CXCR4* improved after treatment with the porous Se@SiO_2 nanocomposite, indicating that the effects of the porous Se@SiO_2 nanocomposite on BMSCs migration may be mediated by the SDF-1/CXCR4 signaling pathway, which plays an important role in controlling BMSCs migration.[34]

The damage of blood vessels after bone fracture can result in hypoxia. On the one hand, hypoxia triggers BMSCs to express BMP-2 and initiate fracture healing; on the other hand, enhanced ROS generation impairs BMP-2 expression, induces BMSCs apoptosis and restricts the osteogenic differentiation of BMSCs, which may ultimately lead to delayed union or nonunion of fracture.[12,35–37] Therefore, reducing oxidative stress and eliminating excessive ROS may promote bone fracture.[38,39]

Se is of great significance to human health, and selenoenzymes, such as glutathione peroxidases and selenoprotein P, play an important role in protecting cells against oxidative stress.[40] Se deficiency may result in a deficient antioxidative capacity in some illnesses[41] and in the case of multiple severe injuries.[42] In addition, Se is essential in bone health, as best reflected by Kashin–Beck disease,[43,44] and it has been reported that Se plays a quite important role in the proliferation and differentiation of BMSCs[16,18] and osteoclasts.[19,20] Therefore, the application of Se in fracture healing is of great importance.

However, too much Se potentially induces harmful effects on health,[21] and considering the narrow margin between safety and toxicity, the harmful levels of excess Se and the safe upper limit of Se have been disputed.[22] Although, Se at the nanoscale (nano-Se) can reduce the risk of Se toxicity,[45] it is not enough to meet the

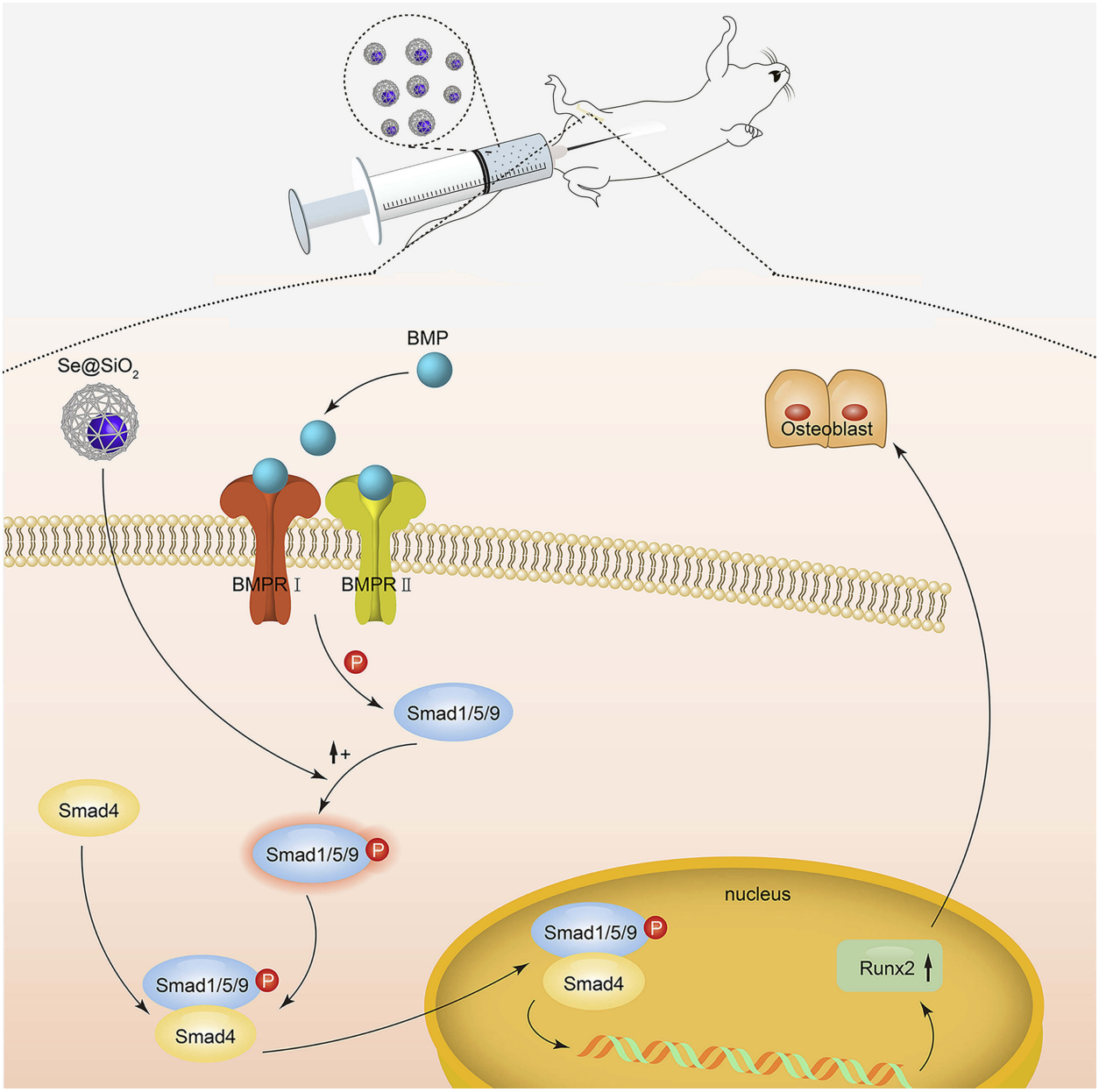

Figure 8 Mechanism of porous Se@SiO_2 nanocomposites to promote osteogenic differentiation of BMSCs and protect BMSCs against H_2O_2-induced inhibition of osteogenic differentiation.

requirement of long-term use.[29] An advantage of the porous Se@SiO_2 nanocomposite is that it can slowly and persistently release a beneficial amount of Se. Our results indicated that the release rate of Se was rapid on the first day and gradually slowed over the next 9 days at pH 7.4 and 37°C. To simulate the fracture acidic environment, the Se release in pH 5.0 has been studied in our previous study. The results indicated that not much difference was observed between the release of Se quantum dots from porous Se@SiO_2 nanospheres in PBS of pH 7.4 and that of pH 5.0.[29] The controlled release and in vivo stability of the porous Se@SiO_2 nanocomposite provide the characteristics of biosafety and low toxicity. In this study, we confirmed the safety of the porous Se@SiO_2 nanocomposite on BMSCs using the CCK-8 assay. Additionally, our previous study confirmed that administration of the porous Se@SiO_2 nanocomposite did not lead to noticeable damage in major organs, which reflects the safety of the porous Se@SiO_2 nanocomposite in vivo.[46–48] Safety of the porous Se@SiO_2 nanocomposite in vitro and in vivo indicates that the porous Se@SiO_2 nanocomposite may be an ideal material for further use in clinical treatment.

Excessive oxidative stress can induce BMSCs apoptosis.[49–51] DCFH-DA fluorescence intensity assays showed that the porous Se@SiO_2 nanocomposite significantly reduced ROS levels produced by BMSCs under H_2O_2 conditions. We also found that the porous Se@SiO_2 nanocomposite protected BMSCs against apoptosis induced by H_2O_2, as demonstrated by the Annexin V-FITC/PI assay and TUNEL assay. The results of the experiment led to the conclusion that the porous Se@SiO_2 nanocomposite can increase the capacity of BMSCs to withstand ROS damage under oxidative stress.

Excessive oxidative stress may inhibit osteogenic differentiation of BMSCs.[52–54] We found that the porous Se@SiO_2 nanocomposite protected BMSCs against H_2O_2-induced inhibition of osteogenic differentiation. ALP is an early marker of osteogenic differentiation.[55] H_2O_2 treatment remarkably reduced ALP activity compared to that of the blank group; however, the porous Se@SiO_2 nanocomposite downregulated ALP activity, indicating that the porous Se@SiO_2 nanocomposite can protect BMSCs against H_2O_2-induced osteogenic inhibition in the early stage of differentiation. Protection of the late stage of osteogenic differentiation was confirmed by Alizarin Red S. Apart from protecting BMSCs against H_2O_2-induced inhibition of osteogenic differentiation, the ALP activity results and Alizarin Red S staining results also indicated that the porous Se@SiO_2 nanocomposite can promote the osteogenic differentiation of BMSCs.

The ability of the porous Se@SiO_2 nanocomposite to promote osteogenic differentiation of BMSCs and to protect BMSCs against H_2O_2-induced inhibition of osteogenic differentiation was further detected by RT-PCR. Compared with the expression levels in the H_2O_2 group, the porous Se@SiO_2 nanocomposite reversed the H_2O_2-suppressed gene expression of *Runx2*, which is an essential master transcription factor for osteogenic differentiation, and the porous Se@SiO_2 nanocomposite also promoted the expression of *Runx2* in the Se@SiO_2 group compared with that in the control group.

Runx2 has a synergistic effect with BMP-induced osteogenic differentiation, and the high expression of Runx2 suggests that the porous Se@SiO_2 nanocomposite effects on BMSCs osteogenic differentiation may be mediated by the BMP/Smad signaling pathway, which is known for its involvement in BMSCs osteogenic differentiation.[56] BMPs are members of the TGF-β superfamily, which are molecules that play an important role in osteogenic differentiation.[57] BMPs first bind to BMP type Ⅱ receptors (BMPR Ⅱ), which phosphorylate the GS region of BMP type Ⅰ receptors (BMPR Ⅰ). Next, activated BMPR Ⅰ phosphorylates Smad1, Smad5 and Smad9 through the GS region and then forms a complex with Smad4, and the complex then translocates into the nucleus.[58] In the nucleus, pSmad can interact with Runx2 to initiate osteogenic differentiation.[10] We confirmed that the effects of the porous Se@SiO_2 nanocomposite on osteogenic differentiation may be mediated by the BMP/Smad signaling pathway synergizing with Runx2.

In addition, we used an open femur fracture model in 8-week-old SD rats to determine whether the porous Se@SiO_2 nanocomposite could accelerate bone fracture healing in vivo. The results showed that the porous Se@SiO_2 nanocomposite accelerated the fracture repair process. The radiographic results qualitatively showed that the porous Se@SiO_2 nanocomposite promoted callus formation and accelerated bone fracture healing. The micro-CT quantitatively exhibited a greater callus BV density in the Se@SiO_2 group than in the blank group.

Conclusions

Our study demonstrated that the porous Se@SiO_2 nanocomposite can promote BMSCs migration through the SDF-1/CXCR4 signaling pathway and protect BMSCs against H_2O_2-induced apoptosis. In addition, the porous Se@SiO_2 nanocomposite can promote BMSCs osteogenic differentiation and protect BMSCs against H_2O_2-induced inhibition of osteogenic differentiation through the BMP/Smad signaling pathway. Runx2, a transcription factor that plays an important role in osteogenic differentiation, participated in this process. Finally, we demonstrated that the porous Se@SiO_2 nanocomposite accelerated bone fracture healing in vivo using a rat open fracture model. In conclusion, our study presents an important finding that can be applied to develop a new therapeutic strategy for patients with bone fractures, and porous Se@SiO_2 nanocomposite may provide clinical benefit for bone tissue engineering.

Abbreviation list

BMSCs, bone marrow mesenchymal stem cells; Se, selenium; H_2O_2, hydrogen peroxide; Runx2, Runt-related transcription factor 2; OCN, osteocalcin; BMP-2, bone morphogenetic protein-2; SDF-1, stromal cell-derived factor-1; CXCR4, CXC chemokine receptor-4; ROS, reactive oxygen species; PI, propidium iodide; ALP, alkaline phosphatase; PVP, polyvinylpyrrolidone; CCK-8, cell counting kit-8; BCA, bicinchoninic acid; TBS, Tris-buffered saline; DCF, dichlorofluorescein; BMD, bone mineral density;

BV, bone volume; TV, tissue volume; BMPR Ⅰ, BMP type Ⅰ receptors; BMPR Ⅱ, BMP type Ⅱ receptors.

Acknowledgments

This work was supported by the National Natural Science Foundation of China [grant number 71432007] and Medical-Engineering Funding of Shanghai Jiao Tong University [grant number ZH2018QNA20].

Disclosure

The authors report no conflicts of interest in this work.

References

1. Balogh ZJ, Reumann MK, Gruen RL, et al. Advances and future directions for management of trauma patients with musculoskeletal injuries. *Lancet (London, England)*. 2012;380(9847):1109–1119. doi:10.1016/S0140-6736(12)60991-X
2. Nakamura A, Akahane M, Shigematsu H, et al. Cell sheet transplantation of cultured mesenchymal stem cells enhances bone formation in a rat nonunion model. *Bone*. 2010;46(2):418–424. doi:10.1016/j.bone.2009.08.048
3. Kallai I, van Lenthe GH, Ruffoni D, et al. Quantitative, structural, and image-based mechanical analysis of nonunion fracture repaired by genetically engineered mesenchymal stem cells. *J Biomech*. 2010;43(12):2315–2320. doi:10.1016/j.jbiomech.2010.04.031
4. Horwitz EM, Prockop DJ, Fitzpatrick LA, et al. Transplantability and therapeutic effects of bone marrow-derived mesenchymal cells in children with osteogenesis imperfecta. *Nat Med*. 1999;5(3):309–313. doi:10.1038/6529
5. Cancedda R, Bianchi G, Derubeis A, Quarto R. Cell therapy for bone disease: a review of current status. *Stem Cells*. 2003;21(5):610–619. doi:10.1634/stemcells.21-5-610
6. Atashi F, Modarressi A, Pepper MS. The role of reactive oxygen species in mesenchymal stem cell adipogenic and osteogenic differentiation: a review. *Stem Cells Dev*. 2015;24(10):1150–1163. doi:10.1089/scd.2014.0484
7. Marie PJ. Targeting integrins to promote bone formation and repair. *Nat Rev Endocrinol*. 2013;9(5):288–295. doi:10.1038/nrendo.2013.4
8. Guan M, Yao W, Liu R, et al. Directing mesenchymal stem cells to bone to augment bone formation and increase bone mass. *Nat Med*. 2012;18(3):456–462. doi:10.1038/nm.2665
9. Yao W, Lay YE, Kot A, et al. Improved mobilization of exogenous mesenchymal stem cells to bone for fracture healing and sex difference. *Stem Cells*. 2016;34(10):2587–2600. doi:10.1002/stem.2433
10. Takarada T, Nakazato R, Tsuchikane A, et al. Genetic analysis of Runx2 function during intramembranous ossification. *Development*. 2016;143(2):211–218. doi:10.1242/dev.128793
11. Schussler SD, Uske K, Marwah P, et al. Controlled release of vanadium from a composite scaffold stimulates mesenchymal stem cell osteochondrogenesis. *Aaps J*. 2017;19(4):1017–1028. doi:10.1208/s12248-017-0073-9
12. Muinos-Lopez E, Ripalda-Cemborain P, Lopez-Martinez T, et al. Hypoxia and reactive oxygen species homeostasis in mesenchymal progenitor cells define a molecular mechanism for fracture nonunion. *Stem Cells*. 2016;34(9):2342–2353. doi:10.1002/stem.2399
13. Wang H, Wei W, Zhang SY, et al. Melatonin-selenium nanoparticles inhibit oxidative stress and protect against hepatic injury induced by bacillus calmette-guerin/lipopolysaccharide in mice. *J Pineal Res*. 2005;39(2):156–163. doi:10.1111/j.1600-079X.2005.00231.x
14. Wang J, Liu Z, He X, et al. Selenium deficiency induces duodenal villi cell apoptosis via an oxidative stress-induced mitochondrial apoptosis pathway and an inflammatory signaling-induced death receptor pathway. *Metallomics Integr Biometal Sci*. 2018;10:1390.
15. Sheng Y, Liu G, Wang M, Lv Z, Du P. A selenium polysaccharide from Platycodon grandiflorum rescues PC12 cell death caused by H2O2 via inhibiting oxidative stress. *Int J Biol Macromol*. 2017;104:393–399. doi:10.1016/j.ijbiomac.2017.06.052
16. Zeng H, Cao JJ, Combs GF Jr. Selenium in bone health: roles in antioxidant protection and cell proliferation. *Nutrients*. 2013;5(1):97–110. doi:10.3390/nu5010097
17. Cao JJ, Gregoire BR, Zeng H. Selenium deficiency decreases antioxidative capacity and is detrimental to bone microarchitecture in mice. *J Nutr*. 2012;142(8):1526–1531. doi:10.3945/jn.111.157040
18. Liu H, Bian W, Liu S, Huang K. Selenium protects bone marrow stromal cells against hydrogen peroxide-induced inhibition of osteoblastic differentiation by suppressing oxidative stress and ERK signaling pathway. *Biol Trace Elem Res*. 2012;150(1–3):441–450. doi:10.1007/s12011-012-9488-4
19. Steinbeck MJ, Kim JK, Trudeau MJ, Hauschka PV, Karnovsky MJ. Involvement of hydrogen peroxide in the differentiation of clonal HD-11EM cells into osteoclast-like cells. *J Cell Physiol*. 1998;176(3):574–587. doi:10.1002/(SICI)1097-4652(199809)176:3<574::AID-JCP14>3.0.CO;2-#
20. Lean JM, Jagger CJ, Kirstein B, Fuller K, Chambers TJ. Hydrogen peroxide is essential for estrogen-deficiency bone loss and osteoclast formation. *Endocrinology*. 2005;146(2):728–735. doi:10.1210/en.2004-1021
21. Srivastava N, Mukhopadhyay M. Green synthesis and structural characterization of selenium nanoparticles and assessment of their antimicrobial property. *Bioprocess Biosyst Eng*. 2015;38(9):1723–1730. doi:10.1007/s00449-015-1413-8
22. Estevez H, Garcia-Lidon JC, Luque-Garcia JL, Camara C. Effects of chitosan-stabilized selenium nanoparticles on cell proliferation, apoptosis and cell cycle pattern in HepG2 cells: comparison with other selenospecies. *Colloids Surf B Biointerfaces*. 2014;122:184–193. doi:10.1016/j.colsurfb.2014.06.062
23. Zhu Y, Deng G, Ji A, et al. Porous Se@SiO2 nanospheres treated paraquat-induced acute lung injury by resisting oxidative stress. *Int J Nanomedicine*. 2017;12:7143–7152. doi:10.2147/IJN.S143192
24. Komori T, Yagi H, Nomura S, et al. Targeted disruption of Cbfa1 results in a complete lack of bone formation owing to maturational arrest of osteoblasts. *Cell*. 1997;89(5):755–764.
25. Wynn RF, Hart CA, Corradi-Perini C, et al. A small proportion of mesenchymal stem cells strongly expresses functionally active CXCR4 receptor capable of promoting migration to bone marrow. *Blood*. 2004;104(9):2643–2645. doi:10.1182/blood-2004-02-0526
26. Shi M, Li J, Liao L, et al. Regulation of CXCR4 expression in human mesenchymal stem cells by cytokine treatment: role in homing efficiency in NOD/SCID mice. *Haematologica*. 2007;92(7):897–904.
27. Deng G, Wang W, Yang C, Gao R, Yang X, Ye X. Shaking improves the whole bone marrow adherent method of purification. *Mol Med Rep*. 2016;13(4):3133–3138. doi:10.3892/mmr.2016.4920
28. Deng GY, Chen CZ, Zhang JJ, et al. Se@SiO_2 nanocomposites attenuate doxorubicin-induced cardiotoxicity through combatting oxidative damage. *Artif Cell Nanomed Biotechnol*. 2018;46:112–121.
29. Liu X, Deng G, Wang Y, et al. A novel and facile synthesis of porous SiO2-coated ultrasmall Se particles as a drug delivery nanoplatform for efficient synergistic treatment of cancer cells. *Nanoscale*. 2016;8(16):8536–8541. doi:10.1039/c6nr02298g
30. Xu L, Huang S, Hou Y, et al. Sox11-modified mesenchymal stem cells (MSCs) accelerate bone fracture healing: sox11 regulates differentiation and migration of MSCs. *FASEB J*. 2015;29(4):1143–1152. doi:10.1096/fj.14-254169

31. Hankenson KD, Gagne K, Shaughnessy M. Extracellular signaling molecules to promote fracture healing and bone regeneration. *Adv Drug Deliv Rev*. 2015;94:3–12. doi:10.1016/j.addr.2015.09.008
32. Kovach TK, Dighe AS, Lobo PI, Cui Q. Interactions between MSCs and immune cells: implications for bone healing. *J Immunol Res*. 2015;2015:752510. doi:10.1155/2015/752510
33. Rharass T, Lucas S, IN ENDOCRINOLOGY: MECHANISMS. Bone marrow adiposity and bone, a bad romance? *Eur J Endocrinol*. 2018;179(4):R165–R182. doi:10.1530/EJE-18-0182
34. Liu X, Duan B, Cheng Z, et al. SDF-1/CXCR4 axis modulates bone marrow mesenchymal stem cell apoptosis, migration and cytokine secretion. *Protein Cell*. 2011;2(10):845–854. doi:10.1007/s13238-011-1097-z
35. Li M, Chen X, Yan J, et al. Inhibition of osteoclastogenesis by stem cell-derived extracellular matrix through modulation of intracellular reactive oxygen species. *Acta Biomater*. 2018;71:118–131. doi:10.1016/j.actbio.2018.03.003
36. Tan J, Xu X, Tong Z, et al. Decreased osteogenesis of adult mesenchymal stem cells by reactive oxygen species under cyclic stretch: a possible mechanism of age related osteoporosis. *Bone Res*. 2015;3:15003. doi:10.1038/boneres.2015.3
37. Li Q, Gao Z, Chen Y, Guan MX. The role of mitochondria in osteogenic, adipogenic and chondrogenic differentiation of mesenchymal stem cells. *Protein Cell*. 2017;8(6):439–445. doi:10.1007/s13238-017-0385-7
38. Li J, Zhang J, Chen Y, Kawazoe N, Chen G. TEMPO-conjugated gold nanoparticles for reactive oxygen species scavenging and regulation of stem cell differentiation. *ACS Appl Mater Interfaces*. 2017;9(41):35683–35692. doi:10.1021/acsami.7b12486
39. Sun W, Qiao W, Zhou B, et al. Overexpression of Sirt1 in mesenchymal stem cells protects against bone loss in mice by FOXO3a deacetylation and oxidative stress inhibition. *Metabolism*. 2018;88:61–71. doi:10.1016/j.metabol.2018.06.006
40. Rayman MP. The importance of selenium to human health. *Lancet (London, England)*. 2000;356(9225):233–241. doi:10.1016/S0140-6736(00)02490-9
41. Alehagen U, Aaseth J. Selenium and coenzyme Q10 interrelationship in cardiovascular diseases–A clinician's point of view. *J Trace Elem Med Biol*. 2015;31:157–162. doi:10.1016/j.jtemb.2014.11.006
42. Zajnudinov ZM, Shabanov AK, Sorin SN, et al. Selenium metabolism in patients with severe multiple trauma. *Anesteziologiya i Reanimatologiya*. 2014(3):68–71.
43. Moreno-Reyes R, Suetens C, Mathieu F, et al. Kashin-Beck osteoarthropathy in rural Tibet in relation to selenium and iodine status. *N Engl J Med*. 1998;339(16):1112–1120. doi:10.1056/NEJM199810153391604
44. Moreno-Reyes R, Egrise D, Boelaert M, Goldman S, Meuris S. Iodine deficiency mitigates growth retardation and osteopenia in selenium-deficient rats. *J Nutr*. 2006;136(3):595–600. doi:10.1093/jn/136.3.595
45. Zhang J, Wang X, Xu T. Elemental selenium at nano size (Nano-Se) as a potential chemopreventive agent with reduced risk of selenium toxicity: comparison with se-methylselenocysteine in mice. *Toxicol Sci*. 2008;101(1):22–31. doi:10.1093/toxsci/kfm221
46. Deng G, Dai C, Chen J, et al. Porous Se@SiO2 nanocomposites protect the femoral head from methylprednisolone-induced osteonecrosis. *Int J Nanomedicine*. 2018;13:1809–1818.
47. Wang H, Zhang J, Yu H. Elemental selenium at nano size possesses lower toxicity without compromising the fundamental effect on selenoenzymes: comparison with selenomethionine in mice. *Free Radic Biol Med*. 2007;42(10):1524–1533. doi:10.1016/j.freeradbiomed.2007.02.013
48. He Y, Chen S, Liu Z, Cheng C, Li H, Wang M. Toxicity of selenium nanoparticles in male Sprague-Dawley rats at supranutritional and nonlethal levels. *Life Sci*. 2014;115(1–2):44–51. doi:10.1016/j.lfs.2014.08.023
49. Liao L, Su X, Yang X, et al. TNF-alpha inhibits FoxO1 by upregulating miR-705 to aggravate oxidative damage in bone marrow-derived mesenchymal stem cells during osteoporosis. *Stem Cells*. 2016;34(4):1054–1067. doi:10.1002/stem.2274
50. Chen CT, Shih YR, Kuo TK, Lee OK, Wei YH. Coordinated changes of mitochondrial biogenesis and antioxidant enzymes during osteogenic differentiation of human mesenchymal stem cells. *Stem Cells*. 2008;26(4):960–968. doi:10.1634/stemcells.2007-0509
51. Lin CH, Li NT, Cheng HS, Yen ML. Oxidative stress induces imbalance of adipogenic/osteoblastic lineage commitment in mesenchymal stem cells through decreasing SIRT1 functions. *J Cell Mol Med*. 2018;22(2):786–796. doi:10.1111/jcmm.13356
52. Watanabe J, Yamada M, Niibe K, et al. Preconditioning of bone marrow-derived mesenchymal stem cells with N-acetyl-L-cysteine enhances bone regeneration via reinforced resistance to oxidative stress. *Biomaterials*. 2018;185:25–38. doi:10.1016/j.biomaterials.2018.08.055
53. Kim JY, Shin KK, Lee AL, et al. MicroRNA-302 induces proliferation and inhibits oxidant-induced cell death in human adipose tissue-derived mesenchymal stem cells. *Cell Death Dis*. 2014;5:e1385. doi:10.1038/cddis.2014.344
54. Wang X, Zhao T, Huang W, et al. Hsp20-engineered mesenchymal stem cells are resistant to oxidative stress via enhanced activation of Akt and increased secretion of growth factors. *Stem Cells*. 2009;27(12):3021–3031. doi:10.1002/stem.230
55. Li K, Shen Q, Xie Y, You M, Huang L, Zheng X. Incorporation of cerium oxide into hydroxyapatite coating protects bone marrow stromal cells against H2O2-induced inhibition of osteogenic differentiation. *Biol Trace Elem Res*. 2018;182(1):91–104. doi:10.1007/s12011-017-1066-3
56. Kang Q, Song WX, Luo Q, et al. A comprehensive analysis of the dual roles of BMPs in regulating adipogenic and osteogenic differentiation of mesenchymal progenitor cells. *Stem Cells Dev*. 2009;18(4):545–559. doi:10.1089/scd.2008.0130
57. Chen D, Zhao M, Mundy GR. Bone morphogenetic proteins. *Growth Factors*. 2004;22(4):233–241. doi:10.1080/08977190412331279890
58. Kugimiya F, Yano F, Ohba S, et al. Mechanism of osteogenic induction by FK506 via BMP/Smad pathways. *Biochem Biophys Res Commun*. 2005;338(2):872–879. doi:10.1016/j.bbrc.2005.10.024